Table II. Summary of *OPTN* variants identified in 218 SALS patients.

| Exon | SNP ID* | Base changes | Annotation | Amino acid changes | Number of cases (Allele frequency) | | Allele frequency (1000 Genomes)** |
|---|---|---|---|---|---|---|---|
| 4 | rs2234968 | c.102G>A | Synonymous | | 3 homozygotes, 59 heterozygotes | (0.149) | 0.182 |
| 4 | Novel | c.147C>T | Synonymous | | 1 homozygote | (0.004) | 0.000 |
| 5 | rs11258194 | c.293T>A | Non-synonymous | p.Met98Lys | 17 heterozygotes | (0.039) | 0.110 |
| 6 | Novel | c.481G>A | Non-synonymous | p.Val161Met | 1 heterozygote | (0.002) | 0.000 |
| 7 | Novel | c.630A>T | Synonymous | | 1 heterozygote | (0.002) | 0.000 |
| 10 | rs523747 | c.964A>G | Non-synonymous | p.Lys322Glu | 218 homozygotes | (1.000) | 1.000 |
| 16 | rs75654767 | c.1634G>A | Non-synonymous | p.Arg545Gln | 13 heterozygotes | (0.030) | 0.028 |

*SNP ID is the single-nucleotide polymorphism identification obtained from dbSNP database.
**The allele frequencies in East Asian populations were obtained from 1000 Genomes Project (http://www.1000genomes.org/).

complex are clustered. We further conducted the mutational analysis of *OPTN* recruiting four additional patients with SALS in the same district. These patients, however, harbored neither the V161M mutation nor any other mutations in *OPTN*.

The clinical features of the patient with the V161M mutation are briefly presented as follows. The patient was a 35-year-old male at the time of diagnosis of ALS, who developed upper extremity weakness for one year. Weakness and atrophy predominantly in upper extremities gradually worsened. Neurological examination at the age of 39 years revealed tongue atrophy and fasciculation, attenuated tendon reflexes and muscle wasting in the upper extremities, and enhanced tendon reflexes in the lower extremities with bilateral extensor plantar reflexes. He became mechanical-ventilator-dependent at the age of 50 years. There was no evidence of parkinsonism or cognitive impairment at the age of 50 years. His medical history included unexplained vision loss of his right eye in his childhood. His father, who also originated from the southernmost part of the Kii Peninsula, was alive and did not show any symptoms indicative of motor neuron disease when the index patient was 35 years old. His mother, who originated from southeastern part of the Kii Peninsula, died of liver cirrhosis, but her age at death was not indicated.

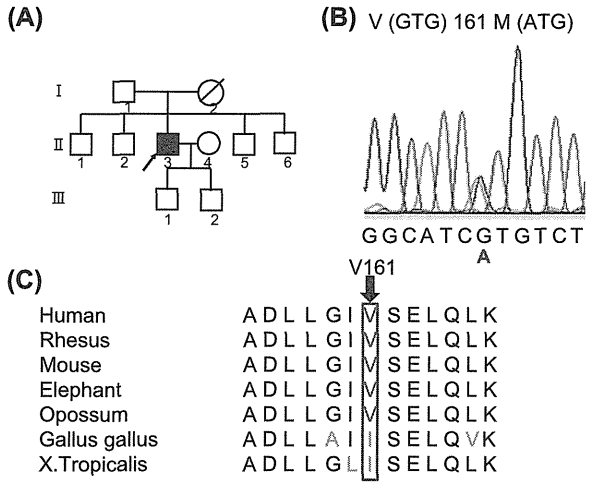


Figure 1. (A) Pedigree chart of patient with V161M variant in *OPTN*. Affected individuals are indicated by filled symbols. The proband is indicated by an arrow. Unaffected individuals are indicated by open symbols. Slashed symbols indicate deceased subjects. Ages at death are shown when information is available. Squares denote male family members and circles denote female family members. (B) Electropherogram of heterozygous *OPTN* c.481G>A (p.Val161Met) point mutation. (C) Conservation of *OPTN* amino acid sequences among different animal species. The valine residue at codon 161 is not necessarily highly conserved among different species (shown in red). Non-conserved amino acids are shown in green.

## Discussion

In this study, we conducted a comprehensive mutational analysis of *OPTN* in a large cohort of Japanese FALS and SALS patients. Among our 35 FALS pedigrees, 17 families had mutations in other causative genes previously reported, as described in Results, and we did not find any causative mutations in *OPTN* in the remaining 18 pedigrees. On the other hand, among the 218 patients with SALS, we identified a patient carrying a novel non-synonymous mutation of *OPTN*.

Previous genetic studies on *OPTN* mutations in different cohorts have demonstrated that the frequencies of *OPTN* mutations are from 0% to 4.35% (pedigree frequency) in FALS (18–23) (Table IIIA). *OPTN* was initially identified as a causative gene for FALS in a consanguineous pedigree through homozygosity mapping followed by sequencing of candidate genes in the homozygous region. In our cohort, autosomal recessive inheritance was suggested in only five of the 35 FALS families, which may account for the fact that we did not identify any causative mutations in *OPTN* in the FALS families. Since the number of families enrolled in this study is limited, further extensive mutational analysis of larger cohorts of FALS will be necessary to establish the genetic epidemiology of FALS patients with *OPTN* mutations.

In our SALS cohort, a novel heterozygous non-synonymous variant, V161M, was identified in a patient. Previous genetic studies on *OPTN* mutations in different cohorts have shown a number of heterozygous missense mutations in SALS patients (20,21) and that the frequencies of *OPTN* mutations are from 0% to 3.54% (case frequency) in SALS (18–23) (Table IIIB). When we assess the implication of the

Table IIIA. Summary of *OPTN* variants identified in FALS patients in previous and present studies.

| Studies | Ethnicity | Variant | Number of pedigrees | Status |
|---|---|---|---|---|
| Maruyama H, et al.[18] | Japanese | exon 5 deletion | 4 | 1 homozygote |
| | | p.Q398X | | 1 homozygote |
| | | p.E478G | | 2 heterozygotes |
| Belzil VV, et al.[19] | European | c.1242+1G>A_insA | 2 | 1 heterozygote |
| | | p.A481V | | 1 heterozygote |
| Del Bo R, et al.[20] | Italian | p.G23X | 2 | 1 heterozygote |
| | | p.K557T | | 1 heterozygote |
| Iida A, et al.[21] | Japanese | p.E478G | 1 | 1 homozygote |
| Millecamps S, et al.[22] | Caucasian | p.R96L | 1 | 1 heterozygote |
| Sugihara K, et al.[23] | Caucasian | None | 0 | |
| Present study | Japanese | None | 0 | |

mutation identified in an isolated case without any family history, we need to carefully consider various possibilities including the possibilities of causative mutation with reduced penetrance and *de novo* mutation. Another possibility is that the variant might not necessarily be associated with a risk of ALS.

Hexanucleotide repeat expansion within the *C9ORF72* gene has very recently been reported to be frequent as a cause of ALS with wider European ancestry. Our recent study on the same cohort indicated that the frequency of the patients with the hexanucleotide repeat expansions is very low (16), suggesting that the result of our molecular epidemiology study of *OPTN* was not substantially affected by that of *C9ORF72* in our Japanese cohort.

Previous studies showed that the clinical phenotypes of patients with *OPTN* mutations are heterogeneous for both age of onset and disease duration, but are characterized by a relatively slow progression, lower-limb onset, and frequent upper motor neuron signs. The relatively slow progression after the onset and the presence of upper motor neuron signs observed in the patient with the V161M variant are consistent with the previous reports (18–23). However, this patient differed from those in previous reports to the extent that the onset site is the upper extremities. Further accumulation of clinical information is essential to delineate the phenotypic spectrum and to illustrate the genotype-phenotype correlations of ALS with *OPTN* mutations.

Of note, the patient originated from the southernmost part of the Kii Penisula including the Koza River, where the prevalence of ALS has been described to be higher than in other areas of Japan (25). Neither the causes of the high prevalence nor the genetic risk factors common to ALS patients in the region have been elucidated. Mutational analysis of four additional ALS patients residing in the same district (Koza River and its vicinity), however, revealed neither the V161M mutation nor other mutations. V161M does not appear to be very common among the patients with ALS in this district.

## Acknowledgements

We thank all patients and their family members for participating in this study. This work was supported in part by KAKENHI (Grant-in-Aid for Scientific Research on Innovative Areas) and Global COE Program from the Ministry of Education, Culture, Sports, Science and Technology of Japan, and a Grant-in-Aid for Research on Intractable Diseases and Comprehensive Research on Disability Health and Welfare from the Ministry of Health, Welfare and Labor, Japan.

***Declaration of interest:*** The authors report no conflicts of interest. The authors alone are responsible for the content and writing of the paper.

Table IIIB. Summary of *OPTN* variants identified in SALS patients in previous and present studies.

| Studies | Ethnicity | Variant | Number of cases | Status |
|---|---|---|---|---|
| Maruyama H, et al.[18] | Japanese | p.Q398X | 1 | 1 homozygote |
| Belzil VV, et al.[19] | European | None | 0 | |
| Del Bo R, et al.[20] | Italian | c.552+1delG | 4 | 1 heterozygote |
| | | p.T282P | | 1 heterozygote |
| | | p.Q314L | | 1 heterozygote |
| | | c.1401+4A>G | | 1 heterozygote |
| Iida A, et al.[21] | Japanese | p.A93P | 2 | 1 heterozygote |
| | | p.E478G | | 1 heterozygote |
| Sugihara K, et al.[23] | Caucasian | None | 0 | |
| Present study | Japanese | p.V161M | 1 | 1 heterozygote |

## References


1. Rosen DR, Siddique T, Patterson D, Figlewicz DA, Sapp P, Hentati A, et al. Mutations in Cu/Zn superoxide dismutase gene are associated with familial amyotrophic lateral sclerosis. Nature. 1993;362:59–62.
2. Hadano S, Hand CK, Osuga H, Yanagisawa Y, Otomo A, Devon RS, et al. A gene encoding a putative GTPase regulator is mutated in familial amyotrophic lateral sclerosis 2. Nat Genet. 2001;29:166–73.
3. Yang Y, Hentati A, Deng HX, Dabbagh O, Sasaki T, Hirano M, et al. The gene encoding alsin, a protein with three guanine-nucleotide exchange factor domains, is mutated in a form of recessive amyotrophic lateral sclerosis. Nat Genet. 2001;29:160–5.
4. Puls I, Jonnakuty C, LaMonte BH, Holzbaur EL, Tokito M, Mann E, et al. Mutant dynactin in motor neuron disease. Nat Genet. 2003;33:455–6.
5. Nishimura AL, Mitne-Neto M, Silva HC, Richieri-Costa A, Middleton S, Cascio D, et al. A mutation in the vesicle-trafficking protein VAPB causes late-onset spinal muscular atrophy and amyotrophic lateral sclerosis. Am J Hum Genet. 2004;75:822–31.
6. Parkinson N, Ince PG, Smith MO, Highley R, Skibinski G, Andersen PM, et al. ALS phenotypes with mutations in CHMP2B (charged multivesicular body protein 2B). Neurology. 2006;67:1074–7.
7. Greenway MJ, Andersen PM, Russ C, Ennis S, Cashman S, Donaghy C, et al. ANG mutations segregate with familial and sporadic amyotrophic lateral sclerosis. Nat Genet. 2006; 38:411–3.
8. Kabashi E, Valdmanis PN, Dion P, Spiegelman D, McConkey BJ, Vande Velde C, et al. TARDBP mutations in individuals with sporadic and familial amyotrophic lateral sclerosis. Nat Genet. 2008;40:572–4.
9. Kwiatkowski TJ Jr, Bosco DA, Leclerc AL, Tamrazian E, Vanderburg CR, Russ C, et al. Mutations in the FUS/TLS gene on chromosome 16 cause familial amyotrophic lateral sclerosis. Science. 2009;323:1205–8.
10. Vance C, Rogelj B, Hortobágyi T, de Vos KJ, Nishimura AL, Sreedharan J, et al. Mutations in FUS, an RNA processing protein, cause familial amyotrophic lateral sclerosis type 6. Science. 2009;323:1208–11.
11. Dion PA, Daoud H, Rouleau GA. Genetics of motor neuron disorders: new insights into pathogenic mechanisms. Nat Rev Genet. 2009;10:769–82.
12. Alexander MD, Traynor BJ, Miller N, Corr B, Frost E, McQuaid S, et al. 'True' sporadic ALS associated with a novel SOD1 mutation. Ann Neurol. 2002;52:680–3.
13. Chiò A, Calvo A, Moglia C, Ossola I, Brunetti M, Sbaiz L, et al. A de novo missense mutation of the FUS gene in a 'true' sporadic ALS case. Neurobiol Aging. 2011;32: 553.e23–6.
14. DeJesus-Hernandez M, Mackenzie IR, Boeve BF, Boxer AL, Baker M, Rutherford NJ, et al. Expanded GGGGCC hexanucleotide repeat in non-coding region of C9ORF72 causes chromosome 9p-linked FTD and ALS. Neuron. 2011;72: 245–56.
15. Renton AE, Majounie E, Waite A, Simon-Sanchez J, Rollinson S, Gibbs JR, et al. A hexanucleotide repeat expansion in C9ORF72 is the cause of chromosome 9p21-linked ALS-FTD. Neuron. 2011;72:257–68.
16. Majounie E, Renton AE, Mok K, Dopper EG, Waite A, Rollinson S, et al. Frequency of the C9orf72 hexanucleotide repeat expansion in patients with amyotrophic lateral sclerosis and frontotemporal dementia: a cross-sectional study. Lancet Neurol. 2012 Mar 9, Epub ahead of print.
17. Deng HX, Chen W, Hong ST, Boycott KM, Gorrie GH, Siddique N, et al. Mutations in UBQLN2 cause dominant X-linked juvenile and adult-onset ALS and ALS/dementia. Nature. 2011;477:211–5.
18. Maruyama H, Morino H, Ito H, Izumi Y, Kato H, Watanabe Y, et al. Mutations of optineurin in amyotrophic lateral sclerosis. Nature. 2010;465:223–6.
19. Belzil VV, Daoud H, Desjarlais A, Bouchard JP, Dupré N, Camu W, et al. Analysis of OPTN as a causative gene for amyotrophic lateral sclerosis. Neurobiol Aging. 2011;32:555. e13–4.
20. Del Bo R, Tiloca C, Pensato V, Corrado L, Ratti A, Ticozzi N, et al. Novel optineurin mutations in patients with familial and sporadic amyotrophic lateral sclerosis. J Neurol Neurosurg Psychiatry. 2011;82:1239–43.
21. Iida A, Hosono N, Sano M, Kamei T, Oshima S, Tokuda T, et al. Optineurin mutations in Japanese amyotrophic lateral sclerosis. J Neurol Neurosurg Psychiatry. 2012;83: 233–5.
22. Millecamps S, Boillée S, Chabrol E, Camu W, Cazeneuve C, Salachas F, et al. Screening of OPTN in French familial amyotrophic lateral sclerosis. Neurobiol Aging. 2011;32: 557.e11–3.
23. Sugihara K, Maruyama H, Kamada M, Morino H, Kawakami H. Screening for OPTN mutations in amyotrophic lateral sclerosis in a mainly Caucasian population. Neurobiol Aging. 2011;32:1923.e9–10.
24. Takahashi Y, Seki N, Ishiura H, Mitsui J, Matsukawa T, Kishino A, et al. Development of a high-throughput microarray-based resequencing system for neurological disorders and its application to molecular genetics of amyotrophic lateral sclerosis. Arch Neurol. 2008;65: 1326–32.
25. Yoshida S, Uebayashi Y, Kihira T, Kohmoto J, Wakayama I, Taguchi S, et al. Epidemiology of motor neuron disease in the Kii Peninsula of Japan, 1989–1993: active or disappearing focus? J Neurol Sci. 1998;155:146–55.

Journal of Histochemistry & Cytochemistry
http://jhc.sagepub.com/

# Enhanced Antigen Retrieval of Amyloid β Immunohistochemistry : Re-evaluation of Amyloid β Pathology in Alzheimer Disease and Its Mouse Model

Hideaki Kai, Ryong-Woon Shin, Koichi Ogino, Hiroyuki Hatsuta, Shigeo Murayama and Tetsuyuki Kitamoto
*J Histochem Cytochem* 2012 60: 761 originally published online 21 July 2012
DOI: 10.1369/0022155412456379

The online version of this article can be found at:
http://jhc.sagepub.com/content/60/10/761

Published by:
SAGE
http://www.sagepublications.com

On behalf of:
HCS
Official Journal of The Histochemical Society



>> Version of Record - Sep 25, 2012

Accepted Manuscript - Jul 21, 2012

What is This?

Journal of Histochemistry & Cytochemistry 60(10) 761–769

DOI: 10.1369/0022155412456379
http://jhc.sagepub.com
SAGE


# Enhanced Antigen Retrieval of Amyloid β Immunohistochemistry: Re-evaluation of Amyloid β Pathology in Alzheimer Disease and Its Mouse Model

**Hideaki Kai, Ryong-Woon Shin, Koichi Ogino, Hiroyuki Hatsuta, Shigeo Murayama, and Tetsuyuki Kitamoto**

Department of Neurological Science, Tohoku University Graduate School of Medicine, Sendai, Japan (HK,R-WS,TK); Qs' Research Institute, Otsuka Pharmaceutical Co. Ltd., Tokushima, Japan (KO); and Department of Neuropathology (The Brain Bank for Aging Research), Tokyo Metropolitan Geriatric Hospital & Institute of Gerontology, Tokyo, Japan (HH,SM).

## Summary

Senile plaques, extracellular deposits of amyloid β peptide (Aβ), are one of the pathological hallmarks of Alzheimer disease (AD). As the standard immunohistochemical detection method for Aβ deposits, anti-Aβ immunohistochemistry combined with antigen retrieval (AR) by formic acid (FA) has been generally used. Here, we present a more efficient AR for Aβ antigen. On brain sections of AD and its mouse model, a double combination of either autoclave heating in EDTA buffer or digestion with proteinase K plus FA treatment reinforced Aβ immunoreactivity. A further triple combination of digestion with proteinase K (P), autoclave heating in EDTA buffer (A), and FA treatment (F), when employed in this order, gave a more enhanced immunoreactivity. Our PAF method prominently visualized various forms of Aβ deposits in AD that have not been clearly detected previously and revealed numerous minute-sized plaques both in AD and the mouse model. Quantification of Aβ loads showed that the AR effect by the PAF method was 1.86-fold (in the aged human brain) and 4.64-fold (in the mouse brain) higher than that by the FA method. Thus, the PAF method could have the potential to be the most sensitive tool so far to study Aβ pathology in AD and its mouse model. (J Histochem Cytochem 60:761–769, 2012)

## Keywords

Alzheimer disease, amyloidβ, antigen retrieval, APP-SL mouse, autoclave heating, formic acid, immunohistochemistry, minute plaque, PAF method, proteinase K

Senile plaques (SPs) and neurofibrillary tangles (NFTs) are two pathological hallmarks that characterize brains afflicted with Alzheimer disease (AD). SPs are extracellular deposits of amyloid β peptide (Aβ) mainly consisting of 40 and 42 residues, which are cleavage products of the amyloid precursor proteins (APPs) (Masters et al. 1985; Kang et al. 1987; Iwatsubo et al. 1994). Aβ is a hydrophobic self-aggregating peptide, and the aggregation of soluble Aβ monomers leads to the composition of insoluble fibrillar polymers, Aβ fibrils. NFTs are intracellular aggregated bundles of a hyperphosphorylated form of the microtubule-associated protein tau (Lee et al. 1991; Ballatore et al. 2007).

Although it is not yet completely elucidated whether SPs and NFTs are the causes or the results of AD onset, the aggregation of Aβ is believed to be implicated in the upper stream of the cascade of AD pathogenesis as a pivotal player in the development of dementia: the amyloid hypothesis (Selkoe 1991; Hardy and Higgins 1992; Hardy and Selkoe 2002). Therefore, the detection of SPs or Aβ deposits with high specificity and sensitivity is essential for elucidating the roles of

Received for publication, June 2, 2012; accepted, June 30, 2012.

Supplementary material for this article is available on the *Journal of Histochemistry & Cytochemistry* Web site at http://jhc.sagepub.com/supplemental.

**Corresponding Author:**
Ryong-Woon Shin, Department of Neurological Science, Tohoku University Graduate School of Medicine, 2-1 Seiryo-machi, Sendai 980-8575, Japan.
Email: rwshin@med.tohoku.ac.jp

parenchymal Aβ deposition and its implication for the pathogenesis of AD as well as its pathological diagnosis. In 1987, our attempt to attain sensitive Aβ immunohistochemistry (IHC) results on formalin-fixed paraffin-embedded (FFPE) tissue sections led to the development of Aβ antigen retrieval (AR) by formic acid (FA) (Kitamoto et al. 1987). This straightforward method dramatically enhances the detection level of Aβ deposits in the AD brain, and since then, anti-AβIHC coupled with FA treatment has been the standard method in the field of Aβ pathology. There is no guarantee, however, that this method can expose all of the existing Aβ deposits without the remains, and we consider that there might be room for improvement of the AR technique. In fact, we had a chance to find irregular and larger forms of Aβ staining, known as fleecy amyloid deposits (Thal et al. 1999), which appear different from the usual SPs in the entorhinal cortex of some AD cases. These structures of Aβ aggregates stained too faintly to be recognized clearly, and we thought that the AR mediated by FA was not efficient enough to detect these Aβ structures. Thus, we tackled the development of a new AR method with a higher efficiency than the conventional FA method. We could substantially improve Aβ IHC by applying two other AR procedures prior to FA treatment. This new AR method enhanced the detection level of numerous SPs and various Aβ deposits that have not been clearly detected by the conventional method and provides a tool to uncover new aspects of Aβ pathology in AD and its mouse models.

## Materials and Methods

### Brain Specimens

Human brain specimens were derived from patients with AD ($n$=11; age range = 63–79 years), non-AD aged individuals with Aβ plaques ($n$=4; age range = 63–77 years), and negative controls for Aβ IHC, who have no family history of AD, including non-AD aged individuals without Aβ plaques ($n$=10; age range = 64–94 years) and healthy young individuals ($n$=6; age range = 21–38 years). For quantification of the Aβ loads, we examined a series of aged human individuals with varying degrees of the Aβ burden ($n$=54; age range = 69–94 years). As transgenic AD mouse models, we used the APP–Swedish/London (SL) lines 7–5 and 7–9, which overexpress human $APP_{Swe/Lon}$ harboring both the Swedish- and London-type mutations. The levels of APP, Aβ40, and Aβ42 in the brain tissues of the mice of line 7–5 are higher than the corresponding levels in the mice of line 7–9 (Shin et al. 2007). The outline of the ages of each of them is as follows: line 7–5 of APP-SL mice aged 6 months ($n$=3), 8 months ($n$=8), 9 months ($n$=2), 10 months ($n$=2), 11 months ($n$=1), 12 months ($n$=4), 13 months ($n$=6), 15 months ($n$=1), 16 months ($n$=5), and 18 months ($n$=1); line 7–9 of APP-SL mice aged 3 months ($n$=3), 6 months ($n$=3), 9 months ($n$=3), 12 months ($n$=2), 13 months ($n$=3), 15 months ($n$=1), 16 months ($n$=2), 18 months ($n$=2), 19 months ($n$=1), and 36 months ($n$=1). The fixation time of brains was 7–13 days with 20% buffered formalin in humans and 3–4 days with 10% buffered formalin in mice. The use of human brains for this work was approved by the Institutional Review Board of Tohoku University Graduate School of Medicine and Tokyo Metropolitan Geriatric Hospital & Institute of Gerontology, and all the animal experiments were done according to the Guidelines for Animal Care and Use at Otsuka Pharmaceutical Co. Ltd.

### AR Procedures

FA pretreatment has been the standard AR method for Aβ IHC. In FA pretreatment, brain tissue sections were incubated in 98% FA (Wako Pure Chemical Industries; Osaka, Japan) for 5 min at room temperature. A challenging trial to largely improve the FA method was performed by combining and applying other AR methods prior to FA treatment. The other AR methods used in this study include heating that employs immersion of tissue sections in 10 mM EDTA (pH 3.0, pH 6.0, and pH 10.0) (Murayama et al. 1999), 0.05% citraconic anhydride (pH 3.0, pH 7.4, and pH 10.0) (Namimatsu et al. 2005), and 0.1 M sodium citrate (pH 3.0, pH 7.2, and pH 10.0) (Bataille et al. 2006) solutions, and distilled water (DW) (pH 3.0 adjusted with hydrochloric acid, pH 7.1, and pH 10.0 adjusted with sodium hydroxide), using an autoclave at 105C or 121C for 10 min (Shin et al. 1991) or using a microwave oven at 90C intermittently but for a total of about 10 min; the proteolytic digestion of tissue sections was performed at 37C for 30 min with 1.0 μg/ml of proteinase K (PK) (Wako Pure Chemical Industries) and 100.0 μg/ml trypsin (Wako Pure Chemical Industries) dissolved in 1.0 mM $CaCl_2$/50 mM Tris buffer (pH 7.6). After each AR treatment, these sections were washed with tap water for at least 5 min and then incubated in DW for at least 5 min.

### Immunostaining

With pretreatment of various combinations of the AR methods, immunostaining was performed as described (Murayama et al. 1999; Shin et al. 2007) using the polyclonal Aβ antibody 4702 (1:1500) (Shin et al. 2007) and monoclonal Aβ antibodies 6E10 (1:2000–4000; Senetek, Maryland Heights, MO) and 4G8 (1:20,000; Senetek). The concentrations of these antibodies were optimized in consideration of both the immunoreactivity and backgrounds of IHC. Brain sections were incubated with primary antibodies in 0.1% Tween-20/Tris-buffered saline (Tris, 50 mM; NaCl, 500 mM; pH 7.6) containing 5% nonfat dried milk for about 15 hr at room temperature. To exclude nonspecific staining unrelated to these polyclonal and monoclonal antibodies, immunostaining was performed with

omission of the antibodies but with all other procedures unchanged in some experiments. Secondary antibodies of EnVision+ system HRP-labeled polymer (Dako; Glostrup, Denmark) were used for the detection of antigen primary mouse or rabbit antibody complexes by diaminobenzidine (DAB). The incubation of the secondary antibodies was for about 1 hr at room temperature. The immunostained brain sections were counterstained with hematoxylin.

### *Microscopes*

The photomicrographs of human and murine samples were captured by an Axiophot2 microscope (Carl Zeiss; Oberkochen, Germany) with Axio Vision version 4.6.3.0 software (Carl Zeiss). In quantification of the Aβ load in the hippocampus of the murine samples, the same system was used in order to assemble sequential micrographs into a single larger one. For measuring the Aβ load, aged human sample photomicrographs were captured by C9600 NanoZoomer (Hamamatsu Photonics; Hamamatsu, Japan) with NDP.view software (Hamamatsu Photonics) because this system is conveniently applicable for capturing and comparing the same regions from serial sections.

### *Measurement of the Area of Aβ Deposits*

In the human brains, we selected three microscopic fields in the fusiform gyrus, which are adequately separated from each other and contain relatively higher Aβ loads. We photographed precisely the same fields in each serial section immunostained following the FA method or PK digestion (P), EDTA autoclaving (A), and FA treatment (F) (in that order; referred to as "PAF") method. All images were from regions of 1408 μm × 1874 μm. In the mouse brains, we selected the whole hippocampus, and its image was constructed from the photomicrographs of 872 μm × 1100 μm by using panorama module of AxioVision version 4.6.3 (Carl Zeiss). All the images were analyzed by ImageJ version 1.43 m (National Institutes of Health; Bethesda, MD) as follows: 1) each raw image was resolved into three images by the color deconvolution setting in hematoxylin and eosin and DAB; 2) the DAB color image among the three resolved images was selected for analysis; 3) the threshold value of the selected image was set to zero as the minimum value and at the optically optimum value set as the maximum value; 4) the thresholded areas of cerebral amyloid angiopathy and artifacts were excluded by selecting and filling them; 5) areas of the Aβ loads (%) to be measured were within a circle (diameter = 1408 μm), the center of which being in the middle of each image in the aged human brains, and within the circumscribed edge of the hippocampus drawn using the selection tools in the mouse brains; and 6) area fractions of the residual thresholded objects within these selections were measured.

### *Statistical Analyses*

All the statistical analyses were performed with SPSS version 17.0 (SPSS; Chicago, IL).

## Results

### *Development of the Enhanced AR Method for Aβ IHC*

For the development of a more efficient Aβ AR method, our strategy was to modify and reinforce the retrieving effects of FA by applying other AR procedures prior to FA treatment. Such AR procedures included autoclave heating in EDTA buffer (the chelating autoclave method) (Murayama et al. 1999) and digestion with PK. With each of these AR procedures followed by FA treatment or with FA treatment alone, immunostaining using the polyclonal anti-Aβ 4702 antibody was performed on brain tissue sections derived from AD patients and APP-SL line 7–5 mice. In immunostaining using the 4702 antibody with no AR, almost no plaques were detected in the AD brains or only a few in the mouse brains (Suppl. Fig. S1). Thus, this 4702 antibody was conveniently used to easily evaluate the effectiveness of the Aβ AR methods.

Compared to the AR procedures above followed by FA treatment and FA treatment alone, both combinations of AR enhanced the Aβ immunoreactive intensity and increased the loads of Aβ plaques, albeit with low to high enhancing effects (Fig. 1A–C,E–G). However, when we applied heating to the EDTA solution, counterstaining of tissue sections with hematoxylin was remarkably thin compared with counterstaining in the FA only method. Notably, the reversed application of the two AR procedures, that is, application of FA treatment and either autoclave heating in EDTA buffer or digestion with PK in this order, showed limited and almost no enhancement, respectively, compared with the single application of FA treatment (data not shown). These results prompted us to try a triple combination of these three AR procedures. The use of the PAF method produced a remarkably stronger enhancement of Aβ immunoreactivity than the two double combinations above (Fig. 1B–D,F–H). In the triple combinations of the three AR methods in different orders other than that used in the PAF method, varying degrees of tissue damage ensued, especially in human brains. Therefore, we refrained from estimating those triple AR combinations. To confirm that this PAF method is universally applicable to Aβ IHC, we examined other Aβ antibodies including 6E10 (Fig. 2A, B, E, F) and 4G8 (Fig. 2C, D, G, H). All of these antibodies showed enhanced Aβ immunoreactivity following the PAF method compared with the FA method, albeit with varied enhancing effects. Omission of the polyclonal or monoclonal primary antibodies in Aβ IHC with the PAF method totally abolished positive immunostaining (Suppl. Fig. S2),

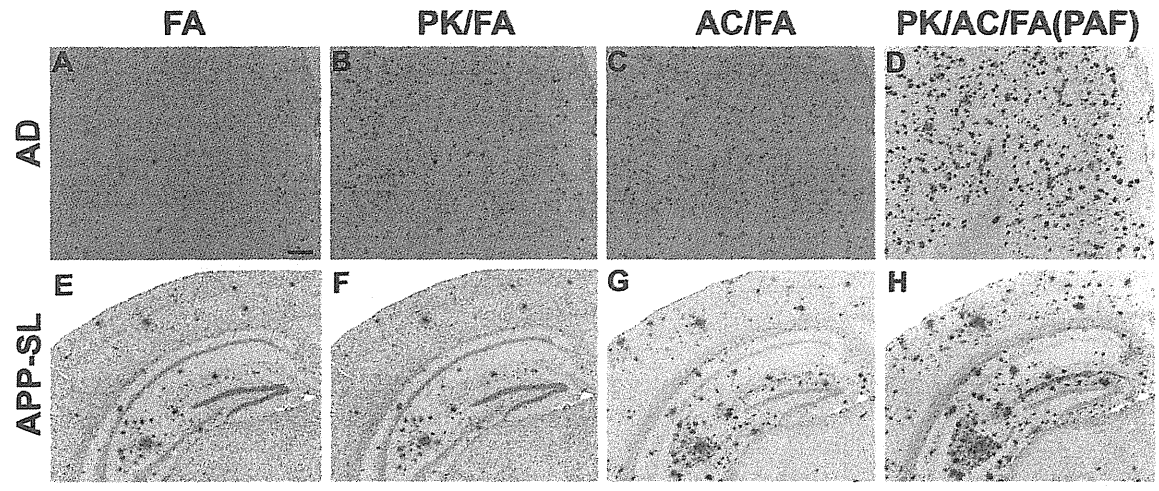


**Figure 1.** Enhancement of formic acid (FA)–mediated amyloid β peptide (Aβ) antigen retrieval. Serial brain tissue sections from a 74-year-old male patient with Alzheimer disease (A–D) and from a 13-month-old amyloid precursor protein–Swedish/London (APP-SL) mouse of line 7–5 (E–H) were immunostained with anti-Aβ antibody 4702 following pretreatment by FA alone (FA) (A, E); combination of digestion with proteinase K and FA (PK/FA) (B, F); combination of autoclave heating in EDTA buffer and FA (AC/FA) (C, G); and triple combination of digestion with proteinase K, autoclave heating in EDTA buffer, and FA (PK/AC/FA) (D, H). Pictures (A–D) are from the temporal cortex. Scale bar = 200 μm (A–H).

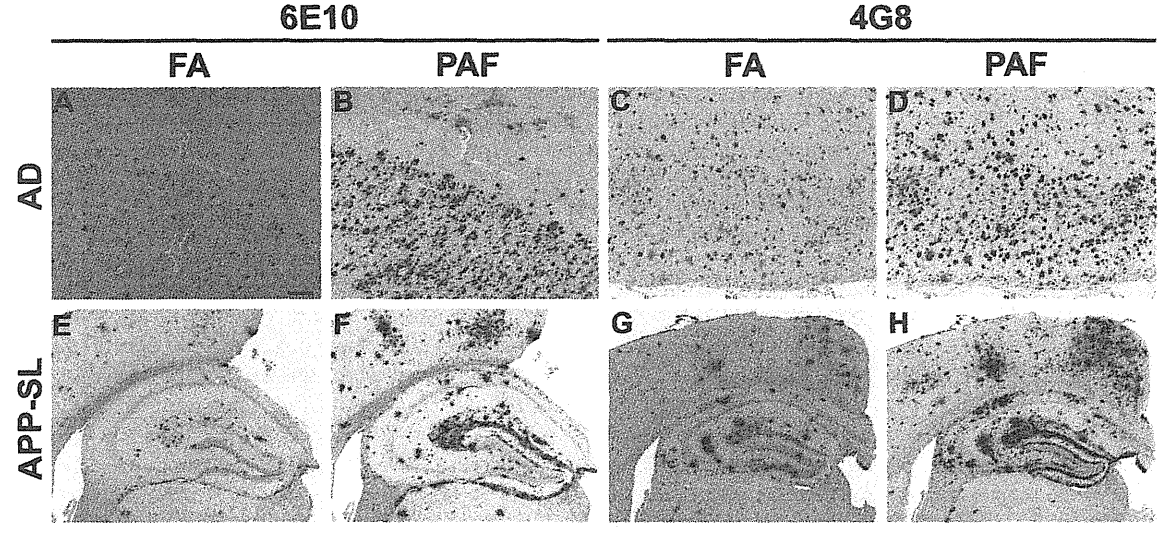


**Figure 2.** General application of the proteinase K digestion (P), EDTA autoclaving (A), and formic acid (FA) treatment (F) (in that order; referred to as "PAF") method in amyloid β peptide (Aβ) immunohistochemistry. Serial (A–B, C–D, E–F, G–H) brain tissue sections from a 74-year-old male patient with Alzheimer disease (the same patient as shown in Fig. 1) (A–D) and a 16-month-old (E, F) and a 15-month-old (G, H) amyloid precursor protein–Swedish/London (APP-SL) mouse of line 7–5 were immunostained with monoclonal anti-Aβ antibodies 6E10 (A, B, E, F) and 4G8 (C, D, G, H) following pretreatment by the FA (A, C, E, G) and PAF methods (B, D, F, H). Pictures are from the cingulate cortex (A, B) and the frontal cortex (C, D). Scale bar = 200 μm (A–H).

which excludes the possibility that immunoreactivity augmented and disclosed following the PAF method was due to nonspecific staining. In addition, no artifactual immunostaining was observed in the brain sections from the normal younger individuals following Aβ IHC assisted by the PAF method (Suppl. Fig. S3).

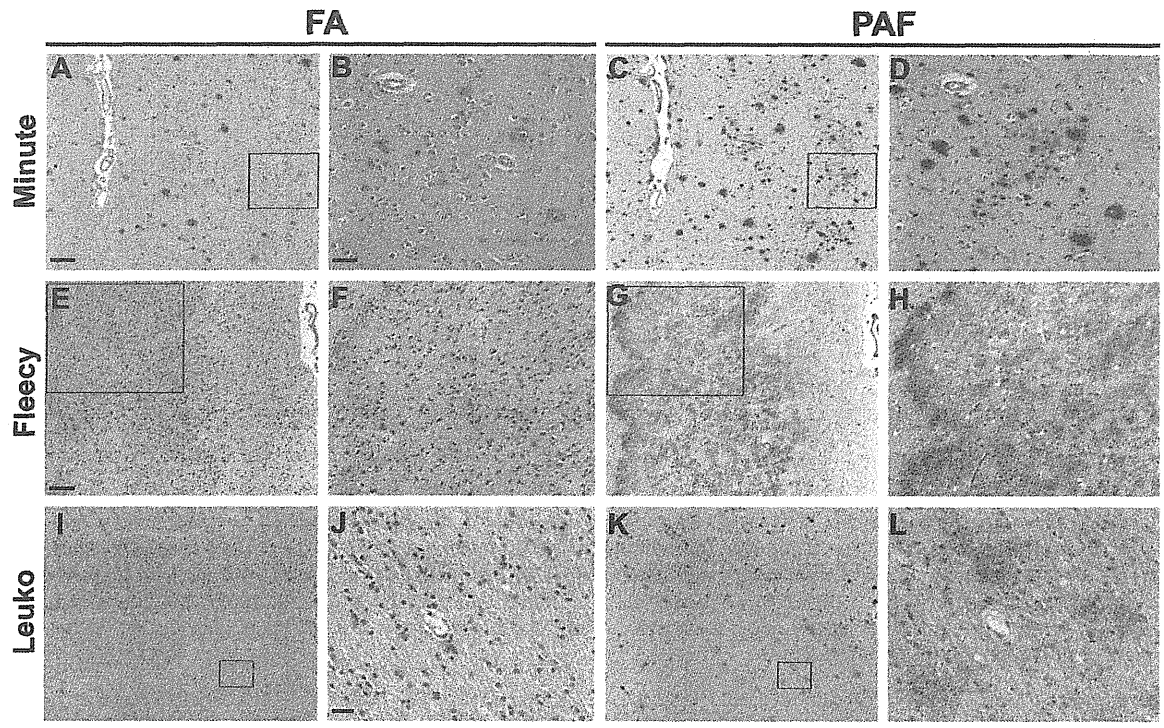


**Figure 3.** Amyloid β peptide (Aβ) pathology of Alzheimer disease (AD) brains enhanced by the proteinase K digestion (P), EDTA autoclaving (A), and formic acid (FA) treatment (F) (in that order; referred to as "PAF") method. Serial brain tissue sections from a 72-year-old female AD patient (the identical patient as shown in Suppl. Fig. S1A,B) (A–D), a 74-year-old male AD patient (the same patient as shown in Fig. 1) (E–H), and a 74-year-old female AD patient (I–L) were immunostained with the 4702 antibody following pretreatment by the FA (A, B, E, F, I, J) and PAF methods (C, D, G, H, K, L). Pictures are from the frontal cortex (A–D), the entorhinal cortex (E–H), and the frontal white matter (I–L). B, D, F, H, J, and L are higher magnification pictures of areas outlined by squares in A, C, E, G, I, and K, respectively. Scale bars = 200μm (A, C, I, K); 50 μm (B, D, F, H); 100μm (E, G); and 20 μm (J, L).

## *IHC Analysis of AD Brains by the PAF Method*

Serial sections of the AD brains pretreated with either the PAF or FA method were immunostained with the anti-Aβ 4702 antibody, analyzed for pathological Aβ deposits, and compared between these two methods (Fig. 3). In the cerebral cortex and hippocampus of the sections pretreated with the PAF method, larger Aβ plaques (diameter > ~15 μm) showed immunoreactive enhancement with an enlarged robust contour, although there was no apparent increase in the number of these larger Aβ plaques. The prominent effect given by the PAF method was the disclosure of numerous minute-sized (diameter < ~15 μm) fine-granular plaques (hereafter referred to as "minute plaques") in these brain regions, which were not evidently detected by the FA method (Figs. 1A, D and 3A–D). Remarkably, the number of these minute plaques increased with elevation of the total Aβ load (data not shown). Thus, all of the AD brains examined by the PAF method contained a much higher load of Aβ plaques in the cerebral cortex and hippocampus than those by the FA method. In the entorhinal cortex adjacent to the subiculum, large and irregular contours of Aβ staining appeared, which were composed of fine- to coarse-granular or diffuse Aβ deposits following the PAF method. These were distributed from near the subpial layer into the deep cortex (Fig. 3G, H), which were reported as fleecy Aβ deposits (Thal et al. 1999). These Aβ deposits were only faintly or not appreciably stained following FA treatment (Fig. 3E, F). In the cerebral white matter, small but significant amounts of Aβ deposits in the diffuse or granular form were previously shown to occur (Wisniewski et al. 1989; Behrouz et al. 1991; Uchihara et al. 1995). The PAF method gave immunoreactive enhancement and revealed larger amounts of granular Aβ deposits in the cerebral white matter (Fig. 3I–L). The PAF method also enhanced Aβ immunoreactivity of ribbon-like infiltration in the subpial layer of the cerebral cortex and that of cerebral amyloid angiopathy in the vessels of the brain (data not shown). Thus, the PAF method dramatically enhanced the detection level of a spectrum of all morphological forms of Aβ deposits.

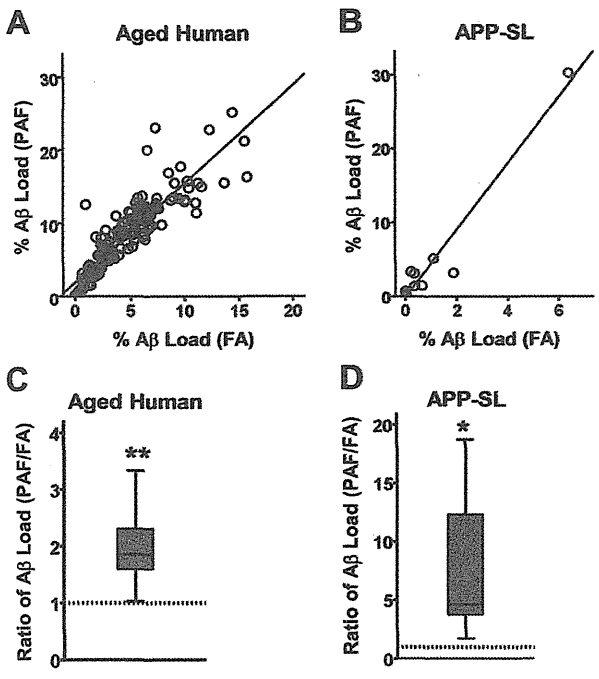


**Figure 4.** Effect of amyloid β peptide (Aβ) antigen retrieval (AR) by the proteinase K digestion (P), EDTA autoclaving (A), and formic acid (FA) treatment (F) (in that order; referred to as "PAF") method over that by the FA method. (A, B) In immunohistochemistry (IHC) with the 4702 antibody, Aβ loads (%) measured in the fusiform cortex of each case from the aged human brains (A) or in the hippocampus of each from the amyloid precursor protein–Swedish/London (APP-SL) mice (B) following the PAF method were plotted against those following the FA method. Significant correlations between the two AR methods were verified both in the aged human brains (Spearman rank correlation coefficient, $r_s$=0.92; $p$=9 × $10^{-69}$) and in the mouse brains ($r_s$=0.80; $p$=0.003). (C, D) The effect of Aβ AR by the PAF method was significantly higher than that by the FA method both in the aged human and in the mouse brains. In IHC with the 4702 antibody, Aβ-loaded areas measured following the PAF method compared with those following the FA method (set at 1.00; the dotted lines) were 1.59-fold at the 25th percentile, 1.86-fold at the 50th percentile, and 2.31-fold at the 75th percentile in the aged human brains (C) and 3.78-fold at the 25th percentile, 4.64-fold at the 50th percentile, and 12.32-fold at the 75th percentile in the mouse brains (D). (C) Ten (≥3.39) and (D) one (92.79) outliers are not shown. **$p$=2 × $10^{-28}$, *$p$=0.01; analyzed by Wilcoxon signed-rank test. $n$=162 from 54 individuals where three regions per case examined (A, C), and $n$=11 (B, D).

## IHC Analysis of the AD Mouse Model by the PAF Method

We examined the brains of the AD APP-SL mice in the same way as for the AD brains. In our previous (Shin et al. 2007) and present studies using conventional Aβ IHC coupled with the FA method, younger APP-SL mice (< ~9 months) showed no occurrence of Aβ deposition, and older mice (≥ ~9 months) exhibited deposition of Aβ plaques that increased its burden with age. Application of Aβ IHC assisted by the PAF method to those younger mice also failed to reveal Aβ deposition. Therefore, in mice showing no evidence of Aβ deposition as evaluated by the FA method, the PAF method did not create any occurrence of Aβ deposition. Thus, these two methods show no difference in their ability to demonstrate the absence of Aβ deposition. In the older mice showing evidence of Aβ deposition, the PAF method was more efficient than the FA method for AR. The enhanced immunoreactive profile was shown to enlarge the sizes and to increase the numbers and immunointensities of Aβ plaques (Figs. 1E,H and 2E–H). Notably, minute Aβ plaques appeared to have a similar morphology as those seen in the AD brains. These minute plaques occur in brain samples containing significant amounts of Aβ burden and prevail dominantly with severity of Aβ burden, as was shown in the AD brain. In 9-month-old APP-SL mice that show an initial appearance of Aβ deposition, Aβ deposits were indiscernible when evaluated by the FA method. These deposits were prominently visualized as distinct Aβ deposits by the PAF method (data not shown). Thus, the PAF method could have an advantage for the retrieval of antigens in Aβ IHC in comparison with the FA method in the AD mouse model as well as humans.

## Efficiency of Aβ AR by the PAF Method

We measured the areas of Aβ deposit loads in the serial sections immunostained with the 4702 antibody following the PAF or FA method, and the total sums of the Aβ-loaded areas per the whole area analyzed were compared between the two methods. In the aged human brains, Aβ deposit loads measured in the fusiform cortex by the PAF method were significantly correlated with those by the FA method ($p$=9 × $10^{-69}$) (Fig. 4A). We compared the ratio of the Aβ deposit area from the PAF method with the ratio from the FA method. The AR effect of the PAF method (Fig. 4C) was significantly higher than that of the FA method (1.86-fold at the median) ($p$=2 × $10^{-28}$). In the APP-SL line 7–9 mice, Aβ deposit loads measured in the whole hippocampus by the PAF method were also significantly correlated with those by the FA method ($p$=0.003) (Fig. 4B). The enhancing effect of the PAF method compared with that of the FA method (the ratio as described above in aged human brains) was significantly higher and 4.64-fold at the median ($p$=0.01) (Fig. 4D). Thus, the PAF method produced Aβ deposit loads that were consistently and significantly larger than those produced by the FA method.

## Evaluation of PK versus Trypsin in Enzymatic Digestion and Some Other Solutions in Autoclave Heating

To obtain a more effective enzymatic digestion than PK digestion, we additionally tested trypsin in the double combination of enzymatic digestion and the FA method. Trypsin

digestion, when applied prior to the FA method, produced Aβ immunostaining slightly higher in its intensity than the FA method only. However, its efficacy was comparable to that of PK digestion (Suppl. Fig. S4). To obtain a more effective autoclave heating than that in the solution of 10 mM EDTA (pH 6.0) at 121C, we additionally tested solutions of EDTA (pH 3.0 and pH 10.0), DW (pH 3.0, pH 7.1, and pH 10.0), citraconic anhydride (pH 3.0, pH 7.4, and pH 10.0), and sodium citrate (pH 3.0, pH 7.2, and pH 10.0) as well as temperatures of 90C, 105C, and 121C. Among these different conditions, DW (pH 10.0 and 105C) and sodium citrate (pH 7.2 and 105C) produced high Aβ AR effects. A similar effect was observed for EDTA (pH 6.0 and 121C), although sodium citrate slightly damaged the tissue sections (Suppl. Fig. S5). The triple combinations using additional PK or trypsin digestion as the initial step produced higher Aβ AR effects than each of those double combinations, although heating in sodium citrate solution or basic water damaged the tissue sections. Further nonspecific staining was observed in the brain sections of the APP-SL mice applied by the triple combination of trypsin digestion, EDTA autoclaving, and the FA method (Suppl. Figs. S6 and S7). Thus, the triple combination of 1) PK digestion, 2) autoclave heating in 10 mM EDTA (pH 6.0 and 121C), and 3) FA treatment produced the highest Aβ AR effects without damaging tissue sections or producing nonspecific staining.

## Discussion

The masking of antigens by aldehyde fixatives or by paraffin-embedding procedures is a problem for IHC studies. To overcome this problem, enzymatic digestion, FA treatment, and high-temperature heating have been developed. Among these, FA treatment is the standard method mainly used for Aβ IHC of FFPE brain tissue sections, although it was originally developed for the immunoreactive enhancement of cerebral amyloids (prion protein and Aβ) and systemic amyloids (amyloid A and prealbumin) (Kitamoto et al. 1987). The pretreatment of protein digestion with an enzyme such as trypsin had been used for IHC but only in a limited application (Battifora and Kopinski 1986; Huang et al. 1976; Mepham et al. 1979). In 1991, the advent of the heating AR method was a breakthrough in the field of IHC. Shin et al. (1991) reported that the procedure of hydrated autoclaving uncovers the masked epitopes of the microtubule-associated protein tau, showing that high-temperature heating serves as an efficient AR method. Shi et al. (1991) reported that microwave heating also shows an AR effect by testing a variety of antigens and antibodies, establishing the milestone of AR for FFPE tissue sections. Moreover, Shi et al. (1996) devised the test battery approach, which can efficiently determine the optimum protocols of AR for each antigen by comparing the immunostaining results between different kinds of solutions, temperatures, and pH (O'Leary 2001). As one good example using the test battery approach, it was demonstrated that AR procedures can also be applied to immunoelectron microscopy for amyloid deposits composed of the κ light chain or transthyretin (Rocken and Roessner 1999).

Aβ AR by FA is proposed because of the unfolding of the conformational amyloid polymers and thereby the exposing of Aβ antigens through acidic hydrolysis (Kitamoto et al. 1987). Further, FA is suggested to esterify serine residues in Aβ peptides and to alter the conformation of the amyloid polymers, as nuclear magnetic resonance imaging has revealed (Klunk et al. 1994). On the other hand, the possible mechanisms underlying AR by high-temperature heating are summarized as follows: 1) breaking of aldehyde-induced cross-linkage involving antigenic proteins, 2) extraction of diffusible blocking proteins, 3) precipitation of antigenic proteins, and 4) increased penetration of antibodies with better access to epitopes due to rehydration of the tissue sections (Suurmeijer and Boon 1993). In addition, the application of divalent/trivalent chelators in high-temperature heating removes metal ions that mask antigenic proteins (Murayama et al. 1999; Yamamoto et al. 2002; Shin et al. 2003). If autoclave high-temperature heating with EDTA chelators (Murayama et al. 1999) is then used prior to FA treatment, with the aim of affecting its activity of Aβ AR, it is likely that FA gains permeability through the tissue sections up to the unmasked Aβ fibrils. Similarly, if digestion with PK is applied prior to FA treatment, then proteolytic digestion of blocking proteins that surround Aβ fibrils might occur and unmask and thereby expose them to FA. In short, the procedures of EDTA autoclaving and PK digestion might assist the access of FA to Aβ fibrils, resulting in reinforcement of Aβ AR of FA. Indeed, we demonstrated that the combination of preceding EDTA autoclaving or PK digestion with subsequent FA treatment enhanced the AR effects of FA, and the aforementioned hypotheses might indeed be true. In support of this hypothesis, FA treatment prior to PK digestion or EDTA autoclaving gave no or only a minimally discernible enhancement in Aβ immunoreactivity compared with single FA treatment (data not shown). Our present results, together with other previous studies, show that PK digestion and EDTA autoclaving apparently differ in the mechanisms of the reinforcement of Aβ AR. If both PK digestion and EDTA autoclaving are combined with the FA method, their effects on Aβ AR by FA might be complementary rather than equivalent. Indeed, the triple combination of PK digestion and EDTA autoclaving with FA treatment provided a further stronger enhancement of Aβ AR.

Our results based on the PAF method suggest that previous IHC studies performed by the conventional FA method might have underestimated the quantitative burden of Aβ pathology and that brains with AD and its mouse models produce much more Aβ accumulation than previously assumed. Further, the presence of minute plaques revealed

by the PAF method remains to be clarified for its implication for Aβ pathology of AD and its mouse models. Notably, the molecular layer of the hippocampal dentate gyrus is the brain region that produces larger amounts of the minute plaques in the APP-SL mice than in the aged humans. This observation might explain partly, albeit not totally, why the retrieving effects differ between the human and mouse brains.

This powerful PAF method could reveal numerous SPs and various Aβ deposits that have not been detected so far. Therefore, the PAF method could serve as a sensitive IHC tool to give new insights into Aβ pathology of AD and its mouse models. We speculate that the PAF method may be the Aβ AR method with the highest efficiency so far and could be used in place of the conventional FA method.

## Acknowledgments

We thank H. Kudo and H. Murayama for technical assistance and Daniel Berrar (Tokyo Institute of Technology) for the proofreading of this article and helpful comments.

## Declaration of Conflicting Interests

The authors declared no potential conflicts of interest with respect to the research, authorship, and/or publication of this article.

## Funding

The authors received the following financial support for the research, authorship, and/or publication of this article: This work was partially supported by the Starter Research Subvention of Tohoku University Graduate School of Medicine and Grant-in-Aid for Scientific Research on Innovative Areas (Comprehensive Brain Science Network) from the Ministry of Education, Science, Sports and Culture of Japan.

## References

Ballatore C, Lee VM, Trojanowski JQ. 2007. Tau-mediated neurodegeneration in Alzheimer's disease and related disorders. Nat Rev Neurosci. 8:663–672.

Bataille F, Troppmann S, Klebl F, Rogler G, Stoelcker B, Hofstadter F, Bosserhoff AK, Rummele P. 2006. Multiparameter immunofluorescence on paraffin-embedded tissue sections. Appl Immunohistochem Mol Morphol. 14:225–228.

Battifora H, Kopinski M. 1986. The influence of protease digestion and duration of fixation on the immunostaining of keratins: a comparison of formalin and ethanol fixation. J Histochem Cytochem. 34:1095–1100.

Behrouz N, Defossez A, Delacourte A, Mazzuca M. 1991. The immunohistochemical evidence of amyloid diffuse deposits as a pathological hallmark in Alzheimer's disease. J Gerontol. 46:B209–B212.

Hardy J, Selkoe DJ. 2002. The amyloid hypothesis of Alzheimer's disease: progress and problems on the road to therapeutics. Science. 297:353–356.

Hardy JA, Higgins GA. 1992. Alzheimer's disease: the amyloid cascade hypothesis. Science. 256:184–185.

Huang SN, Minassian H, More JD. 1976. Application of immunofluorescent staining on paraffin sections improved by trypsin digestion. Lab Invest. 35:383–390.

Iwatsubo T, Odaka A, Suzuki N, Mizusawa H, Nukina N, Ihara Y. 1994. Visualization of A beta 42(43) and A beta 40 in senile plaques with end-specific A beta monoclonals: evidence that an initially deposited species is A beta 42(43). Neuron. 13:45–53.

Kang J, Lemaire HG, Unterbeck A, Salbaum JM, Masters CL, Grzeschik KH, Multhaup G, Beyreuther K, Muller-Hill B. 1987. The precursor of Alzheimer's disease amyloid A4 protein resembles a cell-surface receptor. Nature. 325:733–736.

Kitamoto T, Ogomori K, Tateishi J, Prusiner SB. 1987. Formic acid pretreatment enhances immunostaining of cerebral and systemic amyloids. Lab Invest. 57:230–236.

Klunk WE, Xu CJ, Pettegrew JW. 1994. NMR identification of the formic acid-modified residue in Alzheimer's amyloid protein. J Neurochem. 62:349–354.

Lee VM, Balin BJ, Otvos L Jr., Trojanowski JQ. 1991. A68: a major subunit of paired helical filaments and derivatized forms of normal Tau. Science. 251:675–678.

Masters CL, Simms G, Weinman NA, Multhaup G, McDonald BL, Beyreuther K. 1985. Amyloid plaque core protein in Alzheimer disease and Down syndrome. Proc Natl Acad Sci U S A. 82:4245–4249.

Mepham BL, Frater W, Mitchell BS. 1979. The use of proteolytic enzymes to improve immunoglobulin staining by the PAP technique. Histochem J. 11:345–357.

Murayama H, Shin RW, Higuchi J, Shibuya S, Muramoto T, Kitamoto T. 1999. Interaction of aluminum with PHFtau in Alzheimer's disease neurofibrillary degeneration evidenced by desferrioxamine-assisted chelating autoclave method. Am J Pathol. 155:877–885.

Namimatsu S, Ghazizadeh M, Sugisaki Y. 2005. Reversing the effects of formalin fixation with citraconic anhydride and heat: a universal antigen retrieval method. J Histochem Cytochem. 53:3–11.

O'Leary TJ. 2001. Standardization in immunohistochemistry. Appl Immunohistochem Mol Morphol. 9:3–8.

Rocken C, Roessner A. 1999. An evaluation of antigen retrieval procedures for immunoelectron microscopic classification of amyloid deposits. J Histochem Cytochem. 47:1385–1394.

Selkoe DJ. 1991. The molecular pathology of Alzheimer's disease. Neuron. 6:487–498.

Shi SR, Cote RJ, Yang C, Chen C, Xu HJ, Benedict WF, Taylor CR. 1996. Development of an optimal protocol for antigen retrieval: a 'test battery' approach exemplified with reference to the staining of retinoblastoma protein (pRB) in formalin-fixed paraffin sections. J Pathol. 179:347–352.

Shi SR, Key ME, Kalra KL. 1991. Antigen retrieval in formalin-fixed, paraffin-embedded tissues: an enhancement method for immunohistochemical staining based on microwave oven heating of tissue sections. J Histochem Cytochem. 39:741–748.

Shin RW, Iwaki T, Kitamoto T, Tateishi J. 1991. Hydrated autoclave pretreatment enhances tau immunoreactivity in formalin-fixed normal and Alzheimer's disease brain tissues. Lab Invest. 64:693–702.

Shin RW, Kruck TP, Murayama H, Kitamoto T. 2003. A novel trivalent cation chelator Feralex dissociates binding of aluminum and iron associated with hyperphosphorylated tau of Alzheimer's disease. Brain Res. 961:139–146.

Shin RW, Ogino K, Shimabuku A, Taki T, Nakashima H, Ishihara T, Kitamoto T. 2007. Amyloid precursor protein cytoplasmic domain with phospho-Thr668 accumulates in Alzheimer's disease and its transgenic models: a role to mediate interaction of Abeta and tau. Acta Neuropathol. 113:627–636.

Suurmeijer AJ, Boon ME. 1993. Notes on the application of microwaves for antigen retrieval in paraffin and plastic tissue sections. Eur J Morphol. 31:144–150.

Thal DR, Sassin I, Schultz C, Haass C, Braak E, Braak H. 1999. Fleecy amyloid deposits in the internal layers of the human entorhinal cortex are comprised of N-terminal truncated fragments of Abeta. J Neuropathol Exp Neurol. 58:210–216.

Uchihara T, Kondo H, Akiyama H, Ikeda K. 1995. White matter amyloid in Alzheimer's disease brain. Acta Neuropathol. 90:51–56.

Wisniewski HM, Bancher C, Barcikowska M, Wen GY, Currie J. 1989. Spectrum of morphological appearance of amyloid deposits in Alzheimer's disease. Acta Neuropathol. 78:337–347.

Yamamoto A, Shin RW, Hasegawa K, Naiki H, Sato H, Yoshimasu F, Kitamoto T. 2002. Iron (III) induces aggregation of hyperphosphorylated tau and its reduction to iron (II) reverses the aggregation: implications in the formation of neurofibrillary tangles of Alzheimer's disease. J Neurochem. 82:1137–1147.

REPORT

# The TRK-Fused Gene Is Mutated in Hereditary Motor and Sensory Neuropathy with Proximal Dominant Involvement

Hiroyuki Ishiura,[1] Wataru Sako,[3] Mari Yoshida,[4] Toshitaka Kawarai,[3] Osamu Tanabe,[3,5] Jun Goto,[1] Yuji Takahashi,[1] Hidetoshi Date,[1] Jun Mitsui,[1] Budrul Ahsan,[1] Yaeko Ichikawa,[1] Atsushi Iwata,[1] Hiide Yoshino,[6] Yuishin Izumi,[3] Koji Fujita,[3] Kouji Maeda,[3] Satoshi Goto,[3] Hidetaka Koizumi,[3] Ryoma Morigaki,[3] Masako Ikemura,[7] Naoko Yamauchi,[7] Shigeo Murayama,[8] Garth A. Nicholson,[9] Hidefumi Ito,[10] Gen Sobue,[11] Masanori Nakagawa,[12] Ryuji Kaji,[3,*] and Shoji Tsuji[1,2,13,*]

Hereditary motor and sensory neuropathy with proximal dominant involvement (HMSN-P) is an autosomal-dominant neurodegenerative disorder characterized by widespread fasciculations, proximal-predominant muscle weakness, and atrophy followed by distal sensory involvement. To date, large families affected by HMSN-P have been reported from two different regions in Japan. Linkage and haplotype analyses of two previously reported families and two new families with the use of high-density SNP arrays further defined the minimum candidate region of 3.3 Mb in chromosomal region 3q12. Exome sequencing showed an identical c.854C>T (p.Pro285-Leu) mutation in the TRK-fused gene (*TFG*) in the four families. Detailed haplotype analysis suggested two independent origins of the mutation. Pathological studies of an autopsied patient revealed TFG- and ubiquitin-immunopositive cytoplasmic inclusions in the spinal and cortical motor neurons. Fragmentation of the Golgi apparatus, a frequent finding in amyotrophic lateral sclerosis, was also observed in the motor neurons with inclusion bodies. Moreover, TAR DNA-binding protein 43 kDa (TDP-43)-positive cytoplasmic inclusions were also demonstrated. In cultured cells expressing mutant TFG, cytoplasmic aggregation of TDP-43 was demonstrated. These findings indicate that formation of TFG-containing cytoplasmic inclusions and concomitant mislocalization of TDP-43 underlie motor neuron degeneration in HMSN-P. Pathological overlap of proteinopathies involving TFG and TDP-43 highlights a new pathway leading to motor neuron degeneration.

Hereditary motor and sensory neuropathy with proximal dominant involvement (HMSN-P [MIM 604484]) is an autosomal-dominant disease characterized by predominantly proximal muscle weakness and atrophy followed by distal sensory disturbances.[1] HMSN-P was first described in patients from the Okinawa Islands of Japan, where more than 100 people are estimated to be affected.[2] Two Brazilian HMSN-P-affected families of Okinawan ancestry have also been reported.[3,4]

The disease onset is usually in the 40s and is followed by a slowly progressive course. Painful muscle cramps and abundant fasciculations are observed, particularly in the early stage of the disease. In contrast to the clinical presentations of other hereditary motor and sensory neuropathies (HMSNs) presenting with predominantly distal motor weakness reflecting axonal-length dependence, the clinical presentation of HMSN-P is unique in that it involves proximal predominant weakness with widespread fasciculations resembling those of amyotrophic lateral sclerosis (ALS).[5] Distal sensory loss is accompanied later in the disease course, but the degree of the sensory involvement varies among patients. Neuropathological findings revealed severe neuronal loss and gliosis in the spinal anterior horns and mild neuronal loss and gliosis in the hypoglossal and facial nuclei of the brainstem, which indicates that the primary pathological feature of HMSN-P is a motor neuronopathy involving motor neurons, but not a motor neuropathy involving axons.[1,5] The posterior column, corticospinal tract, and spinocerebellar tract showed loss of myelinated fibers and gliosis. Neuronal loss and gliosis were found in Clarke's nucleus. Dorsal root ganglia showed mild to marked neuronal loss.[1,5] These observations suggest that HMSN-P shares neuropathological findings in part with those observed in familial ALS.[6]

Previous studies on Okinawan kindreds mapped the disease locus to chromosome 3q.[1] Subsequently, we identified two large families (families 1 and 2 in Figure 1A) affected by quite a similar phenotype in the Kansai area of Japan, located in the middle of the main island of Japan and far distant from the Okinawa Islands. We mapped the

[1]Department of Neurology, The University of Tokyo Graduate School of Medicine, 7-3-1 Hongo, Bunkyo-ku, Tokyo 113-8655, Japan; [2]Medical Genome Center, The University of Tokyo Hospital, 7-3-1 Hongo, Bunkyo-ku, Tokyo 113-8655, Japan; [3]Department of Clinical Neuroscience, The Tokushima University Graduate School of Medicine, 3-18-15 Kuramoto-cho, Tokushima 770-8503, Japan; [4]Department of Neuropathology, Institute for Medical Science of Aging, Aichi Medical University, 21 Karimata, Iwasaku, Nagakute-shi, Aichi 480-1195, Japan; [5]Department of Cell and Developmental Biology, University of Michigan Medical School, 109 Zina Pitcher Place, Ann Arbor, MI 48109-2200, USA; [6]Yoshino Neurology Clinic, 3-3-16 Konodai, Ichikawa, Chiba 272-0827, Japan; [7]Department of Pathology, Graduate School of Medicine, The University of Tokyo, 7-3-1 Hongo, Bunkyo-ku, Tokyo 113-8655, Japan; [8]Department of Neuropathology and the Brain Bank for Aging Research, Tokyo Metropolitan Institute of Gerontology, 35-2 Sakae-cho, Itabashi-ku, Tokyo 173-0015, Japan; [9]Molecular Medicine Laboratory and ANZAC Research Institute, University of Sydney, Sydney NSW 2139, Australia; [10]Department of Neurology, Kyoto University Graduate School of Medicine, 54 Kawahara-cho, Shogoin, Sakyo-ku, Kyoto 606-8507, Japan; [11]Department of Neurology, Nagoya University Graduate School of Medicine, 65 Tsurumai-cho, Showa-ku, Nagoya-shi, Aichi 466-0065, Japan; [12]Department of Neurology and Gerontology, Kyoto Prefectural University Graduate School of Medicine, 465, Kajii-cho, Kamigyo-ku, Kyoto 602-0841, Japan; [13]Division of Applied Genetics, National Institute of Genetics, Yata 1111, Mishima, Shizuoka 11-8540, Japan
*Correspondence: tsuji@m.u-tokyo.ac.jp (S.T.), rkaji@clin.med.tokushima-u.ac.jp (R.K.)
http://dx.doi.org/10.1016/j.ajhg.2012.07.014. 

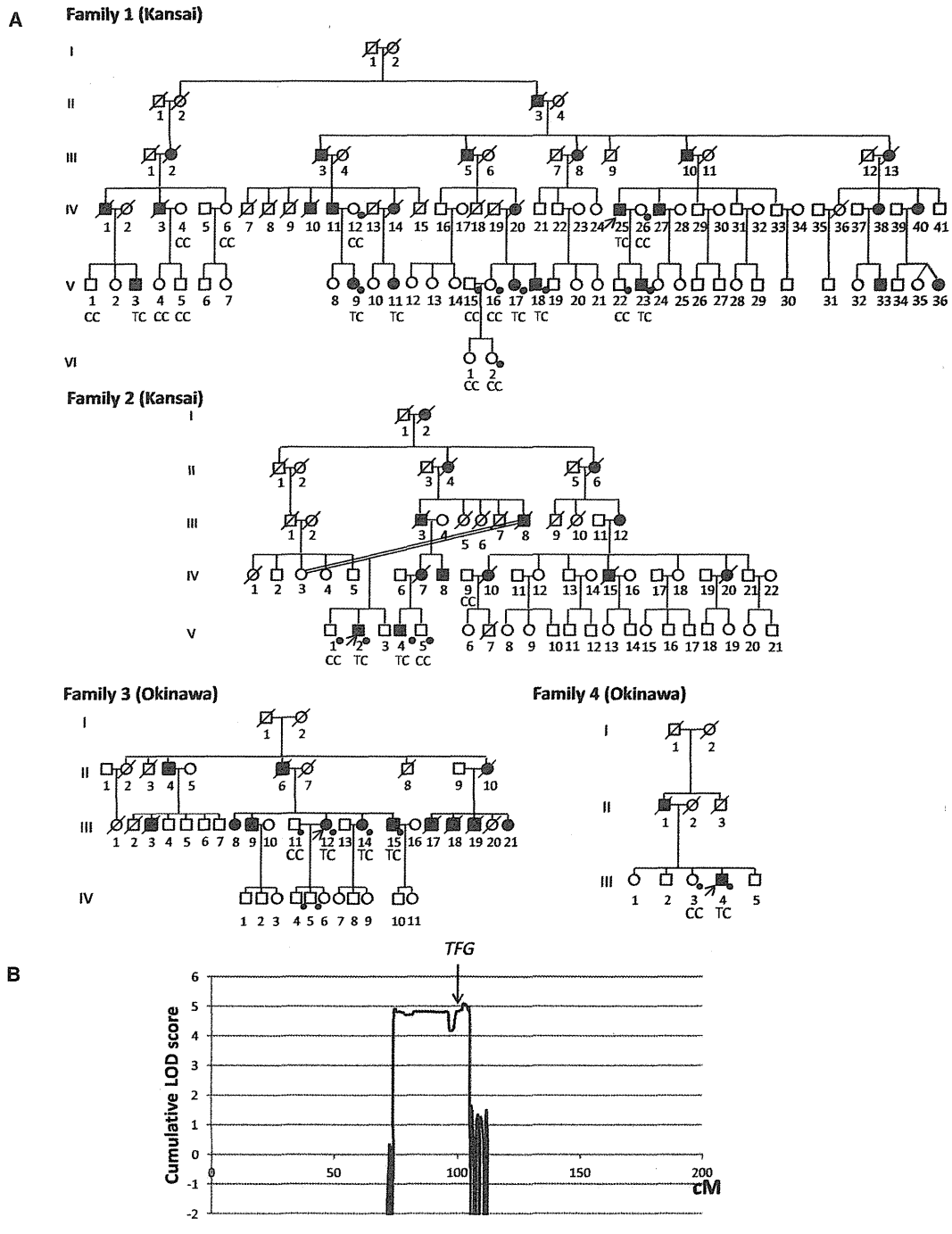


**Figure 1. Pedigree Charts and Linkage Analysis**

(A) Pedigree charts of families 1 and 2 (Kansai kindreds) and families 3 and 4 (Okinawan kindreds) are shown. Squares and circles indicate males and females, respectively. Affected persons are designated with filled symbols. A diagonal line through a symbol represents a deceased person. A person with an arrow is an index patient. Genotypes of *TFG* c.854 are shown in individuals in whom genomic DNA was analyzed. Individuals genotyped with SNP arrays for linkage analysis and haplotype reconstruction are indicated by dots.
(B) Cumulative parametric multipoint LOD scores on chromosome 3 of all the families are shown.

disease locus to chromosome 3q,[7] overlapping with the previously defined locus, which strongly indicates that these diseases are indeed identical.

In addition to the large Kansai HMSN-P-affected families, we found two new Okinawan HMSN-P-affected families (families 3 and 4 in Figure 1A) in our study. In total, 9 affected and 15 unaffected individuals from the Kansai area and four affected and four unaffected individuals from the Okinawa Islands were enrolled in the study. Written informed consent was obtained from

**Table 1. Clinical Characteristics of Patients with HMSN-P from Families 1 and 2 from Kansai and Families 3 and 4 from Okinawa**

| | | Family 3 | | | Family 4 |
|---|---|---|---|---|---|
| | **Families 1 and 2** | **III-12** | **III-14** | **III-15** | **III-4** |
| Age at examination (years) | 40s–50s | 54 | 52 | 50 | 54 |
| Age at onset (years) | 37.5 ± 8 | 44 | 40 | early 20s | 41 |
| Initial symptoms | shoulder dislocation and difficulty walking | proximal leg weakness | painful cramps | painful cramps and fasciculation | painful cramps and calf atrophy |
| **Motor** | | | | | |
| Proximal muscle weakness and atrophy | + | + | mild | + | + |
| Painful cramps | + | + | + | + | + |
| Fasciculations | + | + | + | + | + |
| Motor ability | bedridden after 10–20 years from disease onset | unable to walk; wheelchair | only mild difficulty climbing stairs | walk with effort | unable to walk; wheelchair |
| Bulbar symptoms | − ~ + | − | − | − | − |
| **Sensory** | | | | | |
| Dysesthesia | + | + | mild | + | + |
| Decreased tactile sensation | + | + | − | mild | + |
| Decreased vibratory sensation | + | mild | mild | mild | + |
| **Reflexes** | | | | | |
| Tendon reflexes | diminished | diminished | diminished | diminished | diminished |
| Pathological reflexes | − | − | − | − | − |
| **Laboratory Tests and Electrophysiological Findings** | | | | | |
| Serum creatine kinase level | 270 ± 101 IU/l | 761 IU/l | not measured | 625 IU/l | 399 IU/l |
| Hyperglycemia | 4/13 patients | − | − | − | + |
| Hyperlipidemia | 3/13 patients | + | − | + | + |
| Nerve conduction study | motor and sensory axonal degeneration | motor and sensory axonal degeneration | not examined | not examined | motor and sensory axonal degeneration |
| Needle electromyography | neurogenic changes with fibrillation potentials and positive sharp waves | neurogenic changes with fibrillation potentials and positive sharp waves | not examined | not examined | not examined |

The clinical characteristics of the patients from families 1 and 2 were summarized in accordance with the previous studies.[5,6]

all participants. This study was approved by the institutional review boards at the University of Tokyo and the Tokushima University Hospital. Genomic DNA was extracted from peripheral-blood leukocytes or an autopsied brain according to standard procedures.

The clinical presentations of the patients from the four families are summarized in Table 1 and Table S1, available online. Characteristic painful cramps and fasciculations were noted at the initial stage of the disease in all the patients from the four families. Whereas some of the patients showed painful cramps in their 20s, the ages of onset of motor weakness (41.6 ± 2.9 years old) were quite uniform. These patients presented slowly progressive, predominantly proximal weakness and atrophy with diminished tendon reflexes in the lower extremities. Sensory impairment was generally mild. Indeed, one patient (III-4 in family 4) has been diagnosed with very slowly progressive ALS. Although frontotemporal dementia (FTD) is an occasionally observed clinical presentation in patients with ALS, dementia was not observed in these patients. Laboratory tests showed mildly elevated serum creatine kinase levels. Electrophysiological studies showed similar results in all the patients investigated and revealed a decreased number of motor units with abundant positive sharp waves, fibrillation, and fasciculation potentials. Sensory-nerve action potentials of the sural nerve were lost in the later stage of the disease. All these clinical findings were similar to those described in previous reports.[1,3,4]

To further narrow the candidate region, we conducted detailed genotyping by employing the Genome-Wide Human SNP array 6.0 (Affymetrix). Multipoint parametric linkage analysis and haplotype reconstruction were performed with the pipeline software SNP-HiTLink[8] and Allegro v.2[9] (Figure 1A). In addition to the SNP genotyping, we also used newly discovered polymorphic dinucleotide repeats for haplotype comparison (microsatellite marker 1 [MS1], chr3: 101,901,207–101,901,249; and MS2, chr3: 102,157,749–102,157,795 in hg18) around *TFG* (see Table S2 for primer sequences). The genome-wide linkage study revealed only one chromosome 3 region showing a cumulative LOD score exceeding 3.0 (Figure 1B), confirming the result of our previous study.[7] An obligate recombination event was observed between rs4894942 and rs1104964, thus further refining the telomeric boundary of the candidate region in Kansai families (Figure 2A). The Okinawan families (families 3 and 4) shared an extended disease haplotype spanning 3.3 Mb, consistent with a founder effect reported in the Okinawan HMSN-P-affected families,[1] thus defining the 3.3 Mb region as the minimum candidate region.

We then performed exon capture (Sequence Capture Human Exome 2.1 M Array [NimbleGen]) of the index patient from family 3 and subsequent passively parallel sequencing by using two lanes of GAIIx (100 bp single end [Illumina]) and a one-fifth slide of SOLiD 4 (50 bp single end [Life Technologies]). GAIIx and SOLiD4 yielded 2.60 and 2.76 Gb of uniquely mapped reads,[10] respectively. The average coverages were 29.0× and 26.8× in GAIIx and SOLiD4, respectively (Table S3 and Figure S1). In summary, 175,236 single nucleotide variants (SNVs) and 25,987 small insertions/deletions were called.[11] The numbers of exonic and splice-site variants were 14,189 and 127, respectively. In the minimum candidate region of 3.3 Mb, only 11 exonic SNVs were found, and only one was novel (i.e., not found in dbSNP) and nonsynonymous. Direct nucleotide-sequence analysis confirmed the presence of heterozygous SNV c.854C>T (p.Pro285Leu) in TRK-fused gene (*TFG* [NM_006070.5]) in all the patients from families 3 and 4 (Figure 3A and Figure S2[12]). Intriguingly, direct nucleotide-sequence analysis of all *TFG* exons (see Table S4 for primer sequences) of one patient from each of families 1 and 2 from the Kansai area revealed an identical c.854C>T (p.Pro285Leu) *TFG* mutation cosegregating with the disease (Figure 1A and Figure 3A). The base substitution was not observed in 482 Japanese controls (964 chromosomes), dbSNP, the 1000 Genomes Project Database, or the Exome Sequencing Project Database. Pro285 is located in the P/Q-rich domain in the C-terminal region of TFG (Figure 3B) and is evolutionally conserved (Figure 3C). PolyPhen predicts it to be "probably damaging." Because some of the exonic sequences were not sufficiently covered by exome sequencing (i.e., their read depths were no more than 10×) (Figure S1), direct nucleotide-sequence analysis was further conducted for these exonic sequences (Table S5). However, it did not reveal any other novel nonsynonymous variants, confirming that c.854C>T (p.Pro285Leu) is the only mutation exclusively present in the candidate region of 3.3 Mb. All together, we concluded that it was the disease-causing mutation.

Because we found an identical mutation in both Kansai (families 1 and 2) and Okinawan (families 3 and 4) families, we then compared the haplotypes with the c.854C>T (p.Pro285Leu) mutation in the Kansai and Okinawan families in detail. To obtain high-resolution haplotypes, we included custom-made markers, including MS1 and MS2, and new SNVs identified by our exome analysis, in addition to the high-density SNPs used in the linkage analysis. The two Kansai families shared as long as 24.0 Mb of haplotype, and the two Okinawan families shared 3.3 Mb, strongly supporting a common ancestry in each region. When the haplotypes of the Kansai and Okinawan families were compared, it turned out that these families do not share the same haplotype because the markers nearest to *TFG* are discordant at markers 48.5 kb centromeric and 677 bp telomeric to the mutation within a haploblock (Figure 2B). Although the possibility of rare recombination events just distal to the mutation cannot be completely excluded, as suggested by the population-based recombination map (Figure 2B), these findings strongly support the interpretation that the mutations have independent origins and provide further evidence that *TFG* contains the causative mutation for this disease.

Mutational analyses of *TFG* were further conducted in patients with other diseases affecting lower motor neurons (including familial ALS [n = 18], axonal HMSN [n = 26], and hereditary motor neuropathy [n = 3]) and revealed no mutations in *TFG*, indicating that c.854C>T (p.Pro285Leu) in *TFG* is highly specific to HMSN-P.

In this study, we identified in all four families a single variant that appears to have developed on two different haplotypes. The mutation disrupts the PXXP motif, also known as the Src homology 3 (SH3) domain, which might affect protein-protein interactions. In addition, substitution of leucine for proline is expected to markedly alter the protein's secondary structure, which might substantially compromise the physiological functions of TFG.

By employing the primers shown in Table S6, we obtained full-length cDNAs by PCR amplification of the cDNAs prepared from a cDNA library of the human fetal brain (Clontech). During this process, four species of cDNA were identified (Figure S3A). To determine the relative abundance of these cDNA species, we used the primers shown in Table S7 to conduct fragment analysis of the RT-PCR products obtained from RNAs extracted from various tissues; these primers were designed to discriminate four cDNA species on the basis of the size of the PCR products. The analysis revealed that TFG is ubiquitously expressed, including in the spinal cord and dorsal root ganglia, which are the affected sites of HMSN-P (Figure S3B).

Neuropathological studies were performed in a *TFG*-mutation-positive patient (IV-25 in family 1) who died of

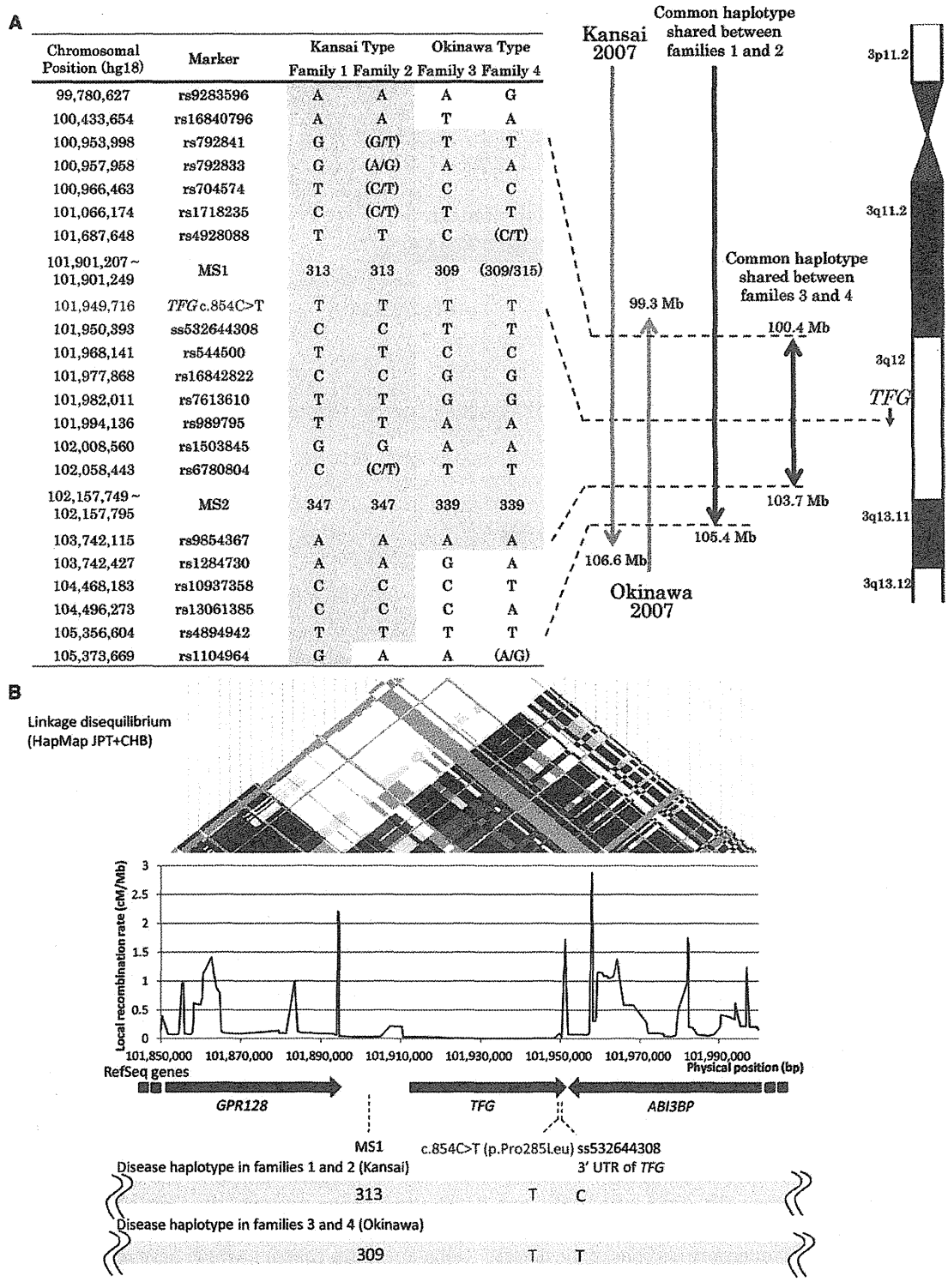


**Figure 2. Haplotype Analysis and Minimum Candidate Region of HMSN-P**

(A) Haplotypes were reconstructed for all the families with the use of SNP array data and microsatellite markers. Previously reported candidate regions are shown as "Kansai 2007" and "Okinawa 2007."[1,6] Because families 1 and 2 are distantly related, an extended shared common haplotype was observed on chromosome 3, as indicated by a previous study.[6] A reassessment of linkage analysis with high-density SNP markers revealed a recombination between rs4894942 and rs1104964 in family 2, thus refining the telomeric boundary of the candidate region in Kansai families (designated as "Common haplotype shared between families 1 and 2). Furthermore, a shared common haplotype (3.3 Mb with boundaries at rs16840796 and rs1284730) between families 3 and 4 was found, defining the minimum candidate region.

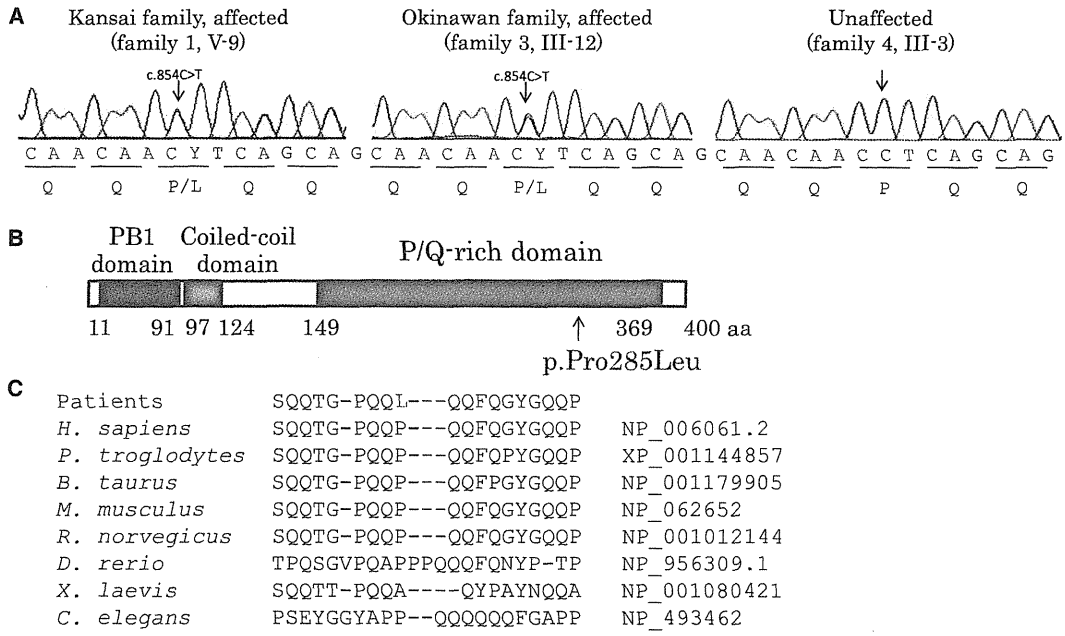


**Figure 3. Identification of Causative Mutation**

(A) Exome sequencing revealed that only one novel nonsynonymous variant is located within the minimum candidate region. Direct nucleotide-sequence analysis confirmed the mutation, c.854C>T (p.Pro285Leu), in *TFG* in both Kansai and Okinawan families. The mutation cosegregated with the disease (Figure 1A).

(B) Schematic representation of TFG isoform 1. The alteration (p.Pro285Leu) detected in this study is shown below.

(C) Cross-species homology search of the partial TFG amino acid sequence containing the p.Pro285Leu alteration revealed that Pro285 is evolutionally conserved among species.

pneumonia at 67 years of age.[5] Immunohistochemical observations employing a TFG antibody (Table S8) revealed fine granular immunostaining of TFG in the cytoplasm of motor neurons in the spinal cord of neurologically normal controls (n = 3; age at death = 58.7 ± 19.6 years old) (Figure 4A). In the HMSN-P patient, in contrast, TFG-immunopositive inclusion bodies were detected in the motor neurons of the facial, hypoglossal, and abducens nuclei and the spinal cord, as well as in the sensory neurons of the dorsal root ganglia, but were not detected in glial cells (Figures 4B–4D). A small number of cortical neurons in the precentral gyrus also showed TFG-immunopositive inclusion bodies (Figure 4E). Serial sections stained with antibodies against ubiquitin or TFG (Figure 4F) and double immunofluorescence staining (Figure 4G) demonstrated that TFG-immunopositive inclusions colocalized with ubiquitin deposition. Inclusion bodies were immunopositive for optineurin in motor neurons of the brainstem nuclei and the anterior horn of the spinal cord,[5] as well as in sensory neurons of the dorsal root ganglia (data not shown). These data strongly indicate that HMSN-P is a proteinopathy involving TFG.

Because HMSN-P and ALS share some clinical characteristics, we then examined whether neuropathological findings of HMSN-P shared cardinal features with those of sporadic ALS.[13–16] Immunohistochemistry with a TDP-43 antibody revealed skein-like inclusions in the remaining motor neurons of the abducens nucleus and the anterior horn of the lumbar cord (Figures 4H–4I). Phosphorylated TDP-43-positive inclusions were also identified in neurons of the anterior horn of the cervical cord and Clarke's nucleus (Figures 4J–4K). In contrast, TFG immunostaining of spinal-cord specimens from four patients with sporadic ALS (their age at death was 72.3 ± 7.4 years old) revealed no pathological staining in the motor neurons (data not shown). Double immunofluorescence staining revealed that many of the TFG-immunopositive round inclusions in the HSMN-P patient were negative for TDP-43 (Figure 4L), whereas a small number of inclusions were positive for both TFG and TDP-43 (Figure 4M). In addition, to investigate morphological Golgi-apparatus changes, which have recently been found in motor neurons of autopsied tissues of ALS patients,[17] we conducted immunohistochemical analysis by using

(B) Disease haplotypes in the Kansai and Okinawan kindreds are indicated below. Local recombination rates, RefSeq genes, and the linkage disequilibrium map from HapMap JPT (Japanese in Tokyo, Japan) and CHB (Han Chinese in Beijing, China) samples are shown above the disease haplotypes. When disease haplotypes of the Kansai and Okinawan kindreds are compared, the markers nearest to *TFG* are discordant at markers 48.5 kb centromeric and 677 bp telomeric to the mutation within a haploblock, strongly supporting the interpretation that the mutations have independent origins.

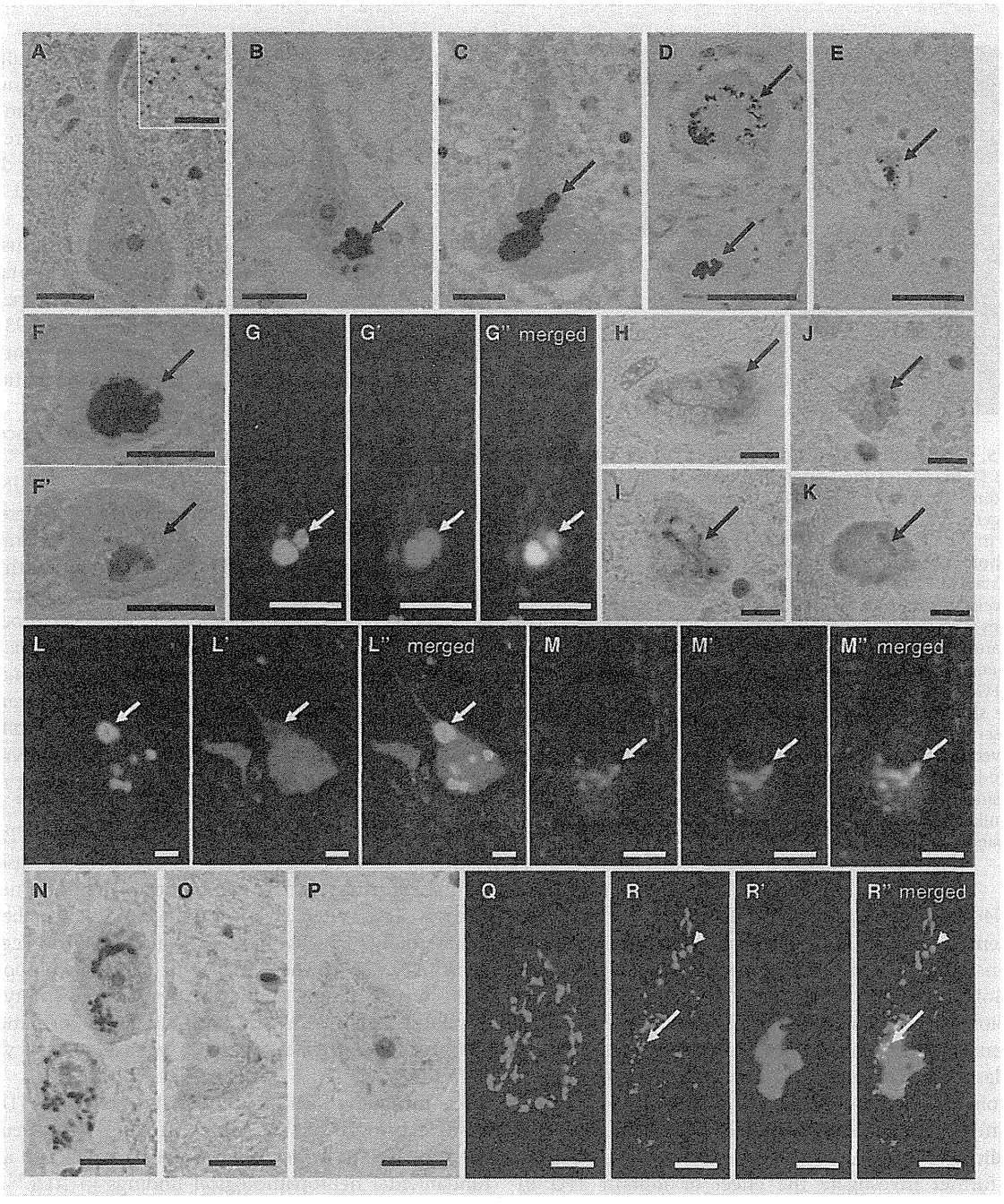


**Figure 4. TFG-Related Neuropathological Findings**

(A) TFG immunostaining (with hematoxylin counterstaining) of a motor neuron in the spinal cord of a neurologically normal control. A high-power magnified photomicrograph (inset) shows fine granular staining of TFG in the cytoplasm. The scale bars represent 20 μm (main panel) and 10 μm (inset).

(B–E) TFG-immunopositive inclusions of the neurons (with hematoxylin counterstaining) in the hypoglossal nucleus (B), anterior horn of the spinal cord (C), dorsal root ganglion (D, arrows), and motor cortex (E, arrow) of the patient with the *TFG* mutation. The scale bars represent 20 μm (B–D) and 50 μm (E).

(F and F′) Serial section analysis of the facial nucleus motor neuron showing an inclusion body colabeled for TFG (F) and ubiquitin (F′). The scale bars represent 20 μm.

(G–G″) Double immunofluorescence microscopy confirming colocalization of TFG (green) and ubiquitin (red) in an inclusion body of a motor neuron in the hypoglossal nucleus. The scale bars represent 20 μm.

(H and I) TDP-43-positive skein-like inclusions in the motor neurons of the abducens nucleus (H) and anterior horn of the lumbar cord (I). The scale bars represent 20 μm.

(J and K) Phosporylated TDP-43-positive inclusion bodies in the cervical anterior horn (J) and Clarke's nucleus (K). The scale bars represent 20 μm.

(L–L″) Round inclusions (arrows) positive for TFG (green) but negative for TDP-43 (red). The scale bars represent 20 μm.